

Electrocatalytic hydrogenation of alkenes with Pd/carbon nanotubes at an oil–water interface

Received: 3 May 2022

Accepted: 17 October 2022

Published online: 22 December 2022

Check for updates

Chenhui Han^{1,3}, Johannes Zenner^{1,2}, Jacob Johny¹, Nicolas Kaeffer¹, Alexis Bordet¹ & Walter Leitner^{1,2}

Electrocatalytic hydrogenation (ECH) produces high-value chemicals from unsaturated organics using water as a hydrogen source. However, ECH is limited by the low solubility of substrates when operated under aqueous conditions, by electrical losses when performed in organic electrolytes and, in general, by low faradaic efficiency and fastidious work-up. Here, we show that a Pickering emulsion compartmenting organic substrates and aqueous electrolytes in different phases enables efficient ECH at the interface. We designed a construct comprising Pd nanoparticles immobilized on positively charged carbon nanotubes that localizes at the interface to act as both emulsion stabilizer and electrocatalyst. Applied to the ECH of styrene, the system delivers ethylbenzene at high faradaic efficiency (95.0%) and mass specific current density ($-148.1 \text{ mA mg}_{\text{Pd}}^{-1}$). The system combines good substrate solubility, high conductivity and simplified product isolation, and has proved applicable to the conversion of various alkenes. This strategy may thus provide alternative solutions to the ECH of substrates with low water solubility, such as bio-oil and bio-crude.

Electron-powered chemical processes are drawing considerable attention because they enable the direct use of renewable energy for the production of high-value chemicals^{1–8}. In particular, electrocatalytic hydrogenation (ECH) has attracted tremendous interest in recent years as a sustainable alternative to hydrogenation processes involving dihydrogen (H_2). ECH offers the possibility of performing low-temperature hydrogenation reactions at ambient temperature and pressure using electricity produced directly from renewable sources to generate hydrogen in situ from water, avoiding the need for H_2 production, storage, transport and handling^{9,10}. Nevertheless, several key limitations prevent the widespread practical application of this technique: low solubility of most organic substrates in aqueous electrolytes; high energy dissipation from ohmic losses in organic electrolytes; low faradaic efficiency (FE); and challenging work-up for product isolation from electrolytes^{11–13}.

Sherbo and colleagues recently partially addressed these limitations¹¹ by modernizing a Pd membrane electrolysis cell^{14,15}. In this case, a Pd membrane acted as a physical separation compartmenting an aqueous electrolyte providing protons and an organic solvent containing the solubilized substrate (Fig. 1a). During the reaction, Pd hydrides were generated electrochemically by the reduction of protons at the interface with the aqueous electrolyte. Permeating through the membrane to the interface with the organic phase, these hydrides could then engage with hydrogenation of substrates (for example, n-hexyne and phenylacetylene)^{11,16,17}. However, moderate reaction rates and FE (20–75%) were typically observed due to the limited membrane area and the limited catalytic activity of bulk Pd¹¹. Moreover, the presence of the Pd membrane prevented ion transfer between electrolyte and organic solvent, blocking the direct electrocatalytic reduction pathway of substrates and resulting in a non-faradaic process in the organic

¹Max Planck Institute for Chemical Energy Conversion, Mülheim an der Ruhr, Germany. ²Institute of Technical and Macromolecular Chemistry, RWTH Aachen University, Aachen, Germany. ³Present address: School of Chemistry and Chemical Engineering, Inner Mongolia University, Hohhot, P. R. China. ✉e-mail: nicolas.kaeffer@cec.mpg.de; alexis.bordet@cec.mpg.de

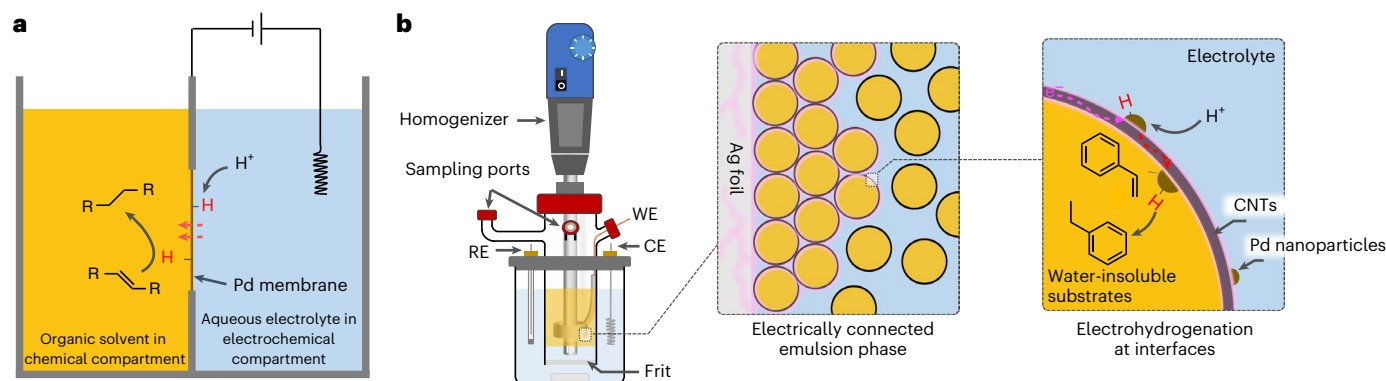


Fig. 1 | ECH in a classical Pd membrane reactor and in our emulsion system.

a. In a Pd membrane reactor, protons of the aqueous phase are electroreduced on the Pd membrane to generate hydrides that diffuse through the membrane and proceed to thermal hydrogenation of the substrate in the organic phase.

b. In the ECH system reported here, the Ag working electrode (WE) used as current collector is located within an oil-in-water Pickering emulsion. The

emulsion is stabilized by molecularly modified CNTs decorated with Pd nanoparticles. The network of emulsion droplets connected to the current collector through electron-conducting CNTs vastly increases the electroactive surface area. At the oil–water interface, electroreduction of protons from the aqueous electrolyte over Pd nanoparticles enables the ECH of water-insoluble alkenes present in the organic phase within emulsion droplets.

compartment. Thus, strategies allowing for a broad application of ECH to organic substrates while providing excellent activity and FE are highly desired but remain challenging.

In this context, we report here the application of Pickering emulsions as a simple and versatile approach to improvement of both the substrate tolerance and efficiency of ECH. Pickering emulsions consist of two immiscible phases, with one being dispersed into the other as micrometre-sized droplets and stabilized at the interface by solid particles¹⁸. Such systems have been applied to catalysis and have shown important benefits for oil–water biphasic reactions by enabling mass transfer between the two phases and involvement of solid particles acting as catalysts at the interface^{19–22}. In ECH, the vast interfaces generated in Pickering emulsions comprising an aqueous electrolyte and a substrate-containing organic phase allow the integration of protons from water into organics in the other phase while eliminating the need for bulk separation (for example, Pd membrane), and thus the associated limitations also. As a case study, we show here that oil-in-water Pickering emulsions stabilized by Pd nanoparticles immobilized on molecularly modified carbon nanotubes (Pd/CNTs) is an efficient electrocatalytic system for alkene ECH (Fig. 1b). Our system outperforms the reported Pd membrane reactor²³ and conventional single-phase cells, with higher ECH current densities achieved at FE of near unity.

Results

Synthesis and characterization of Pd/CNTs

Carbon nanotubes have high electronic conductivity and readily adjustable amphiphilicity through surface functionalization. These two key features make CNTs ideal candidates for ensuring electronic conduction at oil–water interfaces, and we thus selected these materials as emulsion stabilizers and supports for Pd nanoparticles (NPs)^{24,25}. As illustrated in Fig. 2a, commercially available CNTs were treated with a mixture of sulfuric and nitric acid to remove impurity metal ions and generate oxygen-containing groups, such as carboxylic acids, at the surface²⁶. Pretreated CNTs were then molecularly functionalized to tune their surface charge and amphiphilicity. Briefly, histamine was grafted onto CNTs by amide bond formation with surface carboxylic groups, via an acylation procedure²⁷. Then (3-bromopropyl)trimethylammonium bromide was reacted with immobilized histamine moieties to form a quaternary ammonium imidazolium salt. Br[−] ions were exchanged for NTF₂[−] ions to avoid surface poisoning of Pd nanoparticles that would be deposited in the next step (Methods)²⁸. Elemental analysis of the resulting material evidenced around 26 wt% loading of molecular modifier on CNTs, and thermogravimetric analysis indicated thermal

stability at up to 250 °C (Supplementary Table 1 and Supplementary Fig. 1). Zeta-potential measurements showed that molecularly modified CNTs conserve a positively charged surface throughout the whole pH range (named CNTs(+) in the following), while the unmodified sample (treated with acids only) was found to be strongly negatively charged (named CNTs(−); Fig. 2b). CNTs, CNTs(−) and CNTs(+) were characterized by X-ray photoelectron spectroscopy (XPS; Supplementary Fig. 2). The XPS survey spectrum of pristine CNTs shows mostly a C1s core-level contribution (at 284.5 eV) whereas an O1s peak (532.2 eV) is clearly visible in the spectrum of CNTs(−), confirming the introduction of oxygenated functionalities following acid treatment. Following molecular functionalization into CNTs(+), contributions of elements characteristic of the molecular modifier structure (N, F and S) were identified. The final electrocatalysts were obtained by deposition of 5 wt% Pd colloid (around 4.5 nm in diameter; Supplementary Fig. 3) onto the two treated CNT samples, denoted as Pd/CNTs(+) and Pd/CNTs(−), respectively. Characterization of Pd/CNTs(+) by transmission electron microscopy (TEM) showed small and well-dispersed Pd NPs on the CNTs(+) support (Fig. 2c), while elemental mapping of N and S (atoms characteristic of the molecular modifier) by scanning TEM in high-angle annular dark field with energy-dispersive X-ray spectroscopy evidenced homogeneous coverage of the CNT surface by the molecular modifier (Supplementary Fig. 4). In addition, high-resolution XPS spectra of C1s, F1s, N1s and Pd3d levels were recorded for Pd/CNTs(+) (Fig. 2d). The C1s core spectrum is deconvoluted into five components corresponding to different carbonaceous contributions (C=C, C–C, C–O, C=O and π–π*) in the CNTs. However, the C1s spectrum alone did not allow distinguishing of carbons in the backbone of the molecular modifier from the predominant carbon in the CNT structure (Supplementary Fig. 5). Deconvolution of the N1s peak primarily allowed identification of two N-containing species of the modifier chain, namely the C–NH–C group (400.5 eV) and quaternary ammonium (403.1 eV). In addition, the peak at 399.2 eV in the N1s spectrum and the peak at 689.0 eV in the F1s spectrum are characteristic of the NTF₂[−] anion²⁹. These species are characteristic of the molecular modifier, confirming that this is present on the CNTs and retains molecular structure following Pd NPs deposition³⁰.

Emulsions and electrochemical set-up

The electrolysis cell consists of two compartments separated by a glass frit (Fig. 1b). The cathode compartment was filled with a solution of styrene (2 mmol) in cyclohexane (10 ml, oil phase), a 0.5 M H₂SO₄ aqueous electrolyte (10 ml, water phase) and Pd/CNTs (10 mg, 4.7 μmol Pd). This composition corresponds to an aqueous electrolyte:organic

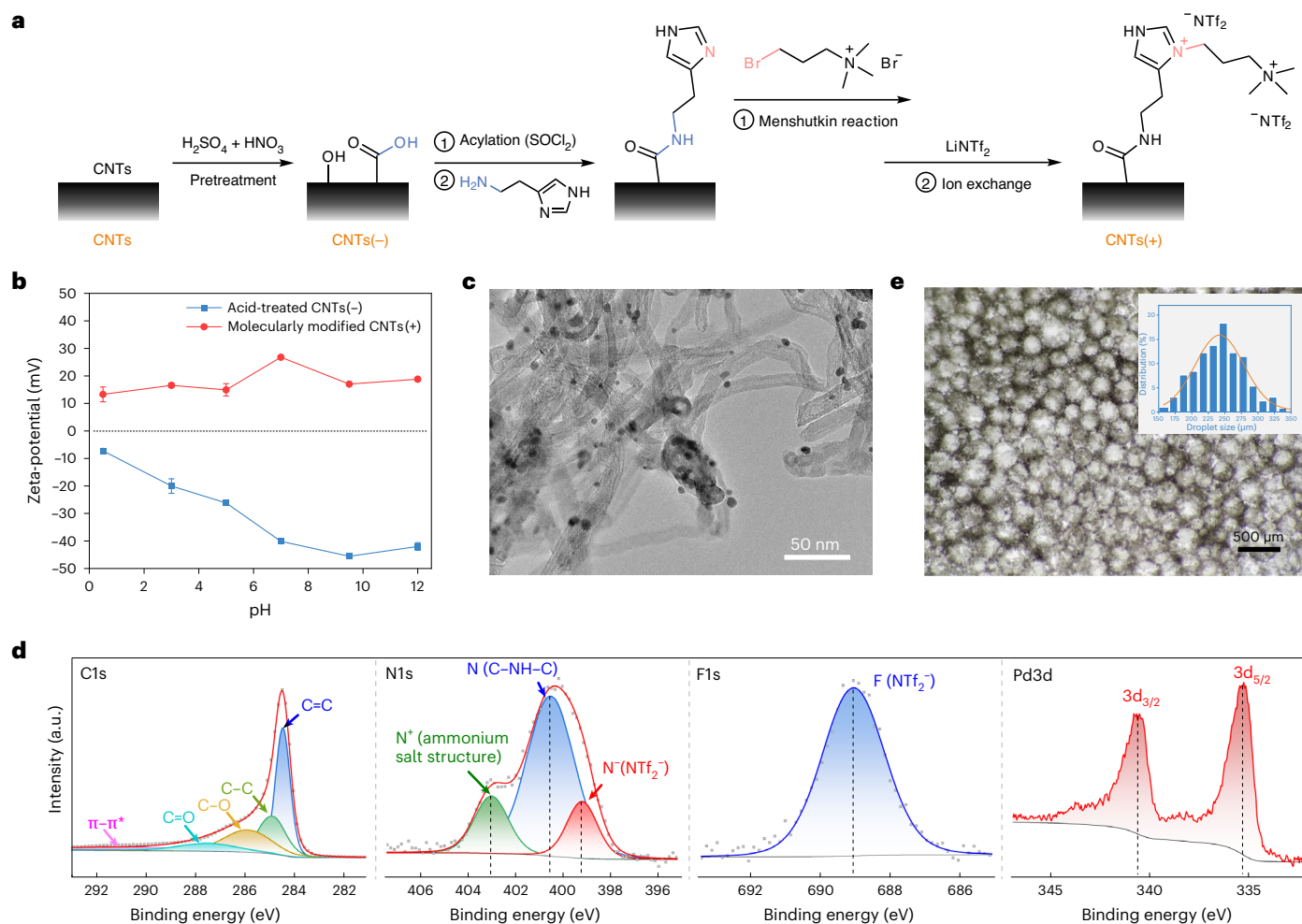


Fig. 2 | Synthesis and characterization of Pd/CNTs. **a**, Pretreatment and molecular modification of CNTs. **b**, Zeta-potential measurements of modified and non-modified CNTs; data presented as mean \pm s.d., as determined from $n = 3$ independent experiments. **c**, TEM image of Pd/CNTs(+). **d**, High-resolution XPS

spectra of C1s, F1s, N1s and Pd3d of Pd/CNTs(+). Spectra were deconvoluted by application of a Shirley-type background. Dots, data points; red line, sum of fits. **e**, Light microscopy image of Pd/CNTs(+)-stabilized Pickering emulsions and corresponding droplet size distribution. a.u., arbitrary units.

solvent volumetric ratio of 1:1, which is typical for Pickering emulsions. A programmable in situ homogenizer was installed on top of the cathode compartment to eliminate a concentration gradient and promote mass transfer in the emulsion phase. Homogenization of mixtures containing Pd/CNTs always successfully resulted in oil-in-water Pickering emulsions. The average droplet size for Pd/CNTs(+)-stabilized emulsions was around 240 μm (Fig. 2e) and was even smaller (around 155 μm) when using Pd/CNTs(-) as stabilizers (Supplementary Fig. 6). Emulsions do not form when using pristine CNTs (Supplementary Fig. 7). Because Ag displays high overpotential for the competing hydrogen evolution reaction (HER)^{31,32}, we selected an annular Ag foil (5 cm²) for introduction into the emulsion phase as the cathodic current collector. We also surmised that the Ag foil surface would be negatively charged under cathodic conditions, thus favouring the adsorption of positively charged emulsion droplet interfaces by coulombic interactions and extending the working surface of the cathode at interfacial Pd/CNTs throughout the emulsion.

Evaluation of the emulsion ECH system

The hydrogenation of styrene to ethylbenzene (EB) was selected as a case study for two reasons: (1) styrene is water insoluble and therefore a good representative of organic compounds with low water solubility; and (2) the unreacted substrate and product can be readily quantified,

thus facilitating the accurate calculation of FE. Linear sweep voltammetry of the emulsion ECH system in the absence of styrene shows the working current for proton reduction in the electrolyte as a function of the applied potential (Fig. 3a). The introduction of styrene provoked a substantial increase in current magnitude at cathodic potentials, which can be attributed to the electrocatalytic conversion of styrene.

The electrocatalytic activities of emulsion systems for styrene ECH were evaluated by electrolysis at -0.65 V (unless otherwise noted) versus the reversible hydrogen electrode (abbreviated V_{RHE} in the following). The reaction was run with intermittent emulsification for 5 s every 5 min until the passage of 2 faradays per mole of styrene, as theoretically required for full conversion into EB. Under these conditions, Pd/CNTs(-)-stabilized emulsions showed a moderate EB yield (72.7%) with -83.5 mA average working current (\bar{j} , passed charge divided by total reaction time) and 72.7% FE to EB (FE_{EB}) (Fig. 3b). The remainder of input charge was mainly consumed in competitive HER ($\text{FE}_{\text{H}_2} = 26.8\%$). In sharp contrast, when the reaction was performed using Pd/CNTs(+)-stabilized emulsions (Fig. 3c), 95.1% EB yield was achieved in 95.0% FE_{EB} and only a trace of H₂ was formed ($\text{FE}_{\text{H}_2} = 1.2\%$). The \bar{j} of -78.0 mA gives a mass partial current density for EB ($j_{\text{Pd}}^{\text{EB}}$) at -148.1 mA $\text{mg}_{\text{Pd}}^{-1}$. Compared with state-of-the-art Pd membrane reactors used in ECH, these results translate into a 30–50% increase in

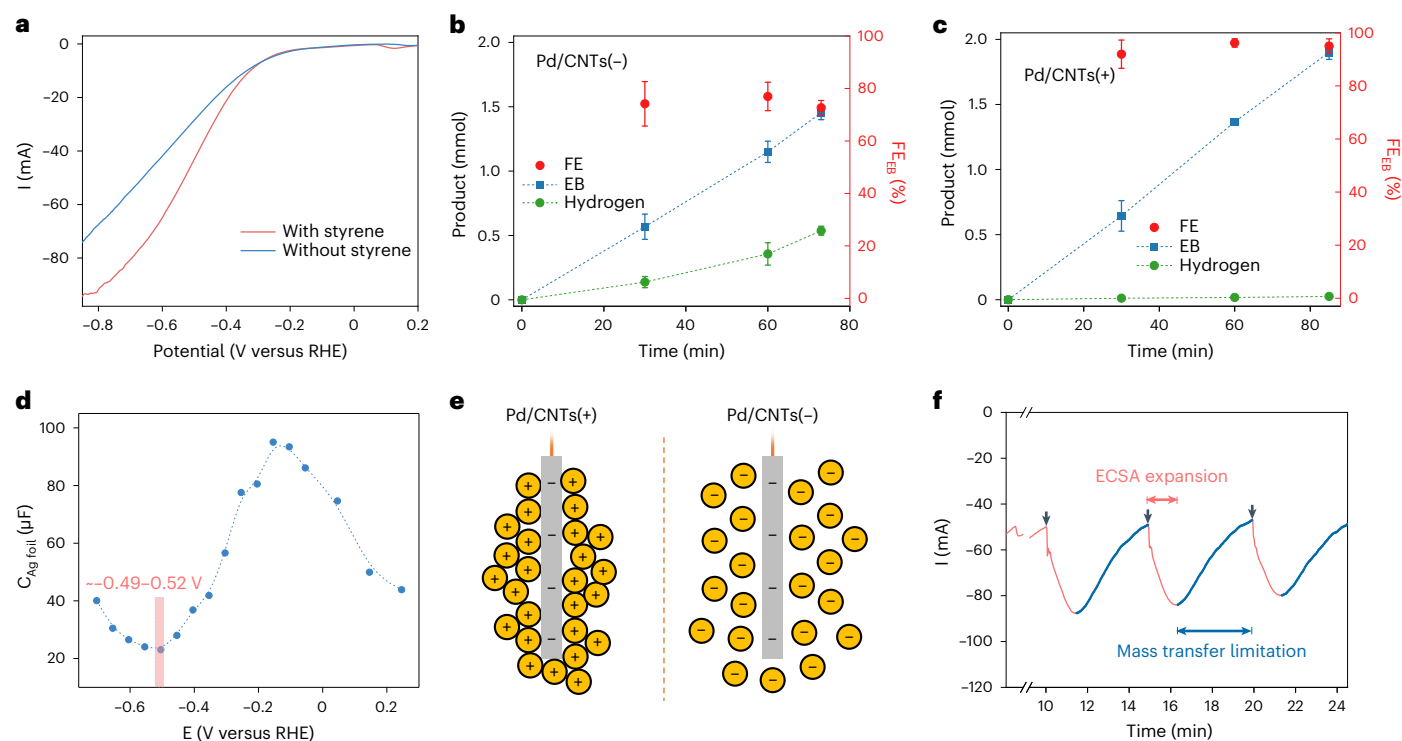


Fig. 3 | Investigation of Pd/CNT-stabilized Pickering emulsions in ECH.

a, Linear sweep voltammetry scans with/without styrene in the oil phase. **b, c**, ECH of styrene using Pd/CNTs(-) (**b**) and Pd/CNTs(+)**(c)**. Reaction conditions: 2 mmol styrene, 10 ml of cyclohexane, 0.5 M H₂SO₄ (75 ml in total), 10 mg of catalyst (4.7 μmol Pd), -0.65 V_{RHE} with iR compensation; emulsified for 5 s every 5 min. The reaction was stopped immediately after a charge of 386 ± 0.5 C had been passed. Data presented as mean ± s.d., as determined

from $n = 3$ independent experiments. **d**, Potential of zero-charge (E_{pzc}) of Ag foil measured by electrochemical impedance spectroscopy. **e**, Schematic illustration of interaction between emulsion droplets and Ag current collector during reaction. **f**, Working current (three typical emulsification-reaction periods are shown) during styrene ECH with Pd/CNTs(+)-stabilized emulsion; black arrows indicate the moment when in situ emulsification was applied. Product yields were determined by GC-FID.

hydrogenation FE, at around tenfold higher Pd mass partial current density²³.

Increasing styrene concentration in the oil phase, from 0.2 to 1.0 M, did not affect emulsion stability and catalytic performance remained excellent (90% yield of EB at 90% FE, $J_{Pd}^{EB} = -187.1 \text{ mA mg}_{Pd}^{-1}$; Supplementary Table 2). Pickering emulsions were found stable even when using pure styrene as the oil phase with no cyclohexane (Supplementary Fig. 8). Under these conditions, the passage of 2 faraday per mole of substrate produced EB at 87% gas chromatography (GC) yield, 88.5% FE and $J_{Pd}^{EB} = -111.6 \text{ mA mg}_{Pd}^{-1}$. Passage of an additional 30% of charge delivered full substrate conversion, from which the product was isolated (5.0 g of isolated product, 65%; Supplementary Fig. 9). Carbon mass balances were closed and no radical coupling products were observed even at elevated concentrations of styrene (Supplementary Fig. 10). However, for more polar substrates such as 4-methoxystyrene, increasing concentration to 1 M resulted in less stable Pickering emulsions and reduced catalytic performance (39.1% yield of 4-ethylanisole at 39.1% FE; $J_{Pd}^{SH2} = -62.8 \text{ mA mg}_{Pd}^{-1}$).

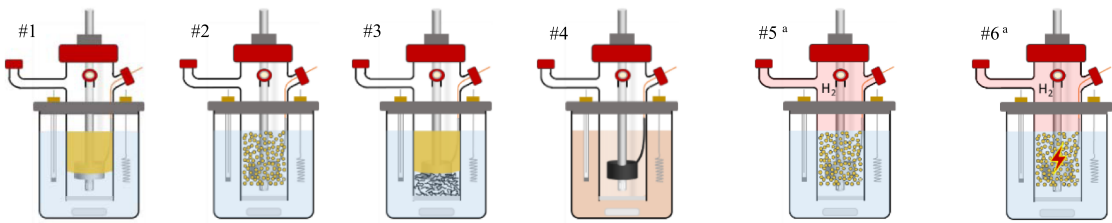
To gain further insight into the variation in performance between systems using Pd/CNTs(-) or Pd/CNTs(+), the surface charge of the current collector (Ag foil) at the working potential (-0.65 V_{RHE}) was investigated. The potential of zero-charge (E_{pzc}) of the Ag foil was measured using electrochemical impedance spectroscopy^{33,34} and was found to be in the range -0.49 to -0.52 V_{RHE} (Fig. 3d). Thus, under capacitive conditions, the surface of the Ag foil is positively charged if the applied potential is higher (that is, less negative) than -0.49 V_{RHE}, but negatively charged if the potential is lower (that is, more negative) than -0.52 V_{RHE}³⁵. At the potential used for electrolysis (-0.65 V_{RHE}) the surface of the Ag foil is then expected to be negatively charged, favouring

the adsorption of positively charged Pd/CNTs(+)-stabilized emulsion droplets that can thus effectively connect to the current collector (Fig. 3e). We propose that, as a result, the electrochemically active surface area (ECSA) extends to the Pd/CNTs(+)-stabilized emulsions which, in turn, fosters catalytic activity and leads to a combination of high working current and FE. Droplet adsorption and electrical connection are probably disfavoured when using non-modified negatively charged Pd/CNTs(-)-catalysts, resulting in a lower electrochemically active area and poor ECH performance. In contrast, at a more positive applied potential of -0.25 V_{RHE}—more positive than E_{pzc} (around -0.5 V_{RHE})—the respective performances are reversed (Supplementary Table 3). Pd/CNTs(-) markedly outperformed Pd/CNTs(+)-stabilized emulsions compared with Pd/CNTs(+)-stabilized emulsions at potentials higher than E_{pzc} (Supplementary Fig. 11). This inversion of behaviour is thus consistent with the fact that interfacial charges are key to the build-up of an extended cathode of large ECSA. These results further support our rationale in using positively charged CNTs(+) to generate an extended cathode at markedly negative applied potential.

The working current gradually increased after each emulsification (Fig. 3f), illustrating expansion of the ECSA due to the continuous connection of emulsion droplets to the current collector during the creaming process (Supplementary Fig. 12). The creaming process is here characterized by the ascent of dispersed droplets to the top of the emulsion due to density differences between the oil and aqueous electrolyte phases. Immediately after emulsification, oil droplets were evenly dispersed throughout the whole emulsion phase. Following creaming, droplets progressively accumulated (without coalescence)

Table 1 | Control experiments

Cell configuration



Brief description	No catalyst (no. 1)	No Pd NPs (no. 2)	No emulsion (no. 3)	Coating catalyst on Ag foil (no. 4)	H ₂ in headspace, no potential (no. 5)	H ₂ in headspace, potential applied (no. 6)
Catalyst	–	CNTs(+)	Pd/CNTs(+)	Pd/CNTs(+)	Pd/CNTs(+) Pd/CNTs(–)	Pd/CNTs(+)
Electrolyte	75 ml of 0.5 M H ₂ SO ₄	75 ml of 0.5 M H ₂ SO ₄	75 ml of 0.5 M H ₂ SO ₄	35 ml of ethanol + 45 ml of 0.5 M H ₂ SO ₄	75 ml of 0.5 M H ₂ SO ₄	75 ml of 0.5 M H ₂ SO ₄
Potential (V _{RHE})	–0.65	–0.65	–0.65	–0.65	NA	–0.65
Charge input (C)	386	375	386	386	NA	193
Reaction time (min)	19	90	82	63	90	47
\bar{j} (mA)	–339.8	–69.5	–78.5	–102.5	NA	–68.6
Styrene conversion (%) ^b	0.1	0.6	22.0	19.5	40.0	42.3
EB yield (%) ^b	0.1	0.6	22.0	19.5	40.0	42.3
FE _{EB} (%)	0.1	0.6	21.9	19.4	NA	98.8
FE _{H₂} (%)	94.9	98.7	76.6	79.4	NA	NA

Reaction conditions: 2 mmol styrene and 10 mg of catalyst (4.7 μmol Pd, when applicable) were used in all cases. All reactions were conducted at room temperature and were stopped on reaching 386 ± 0.5 C or after 90 min (except for no. 6), whichever came first. In situ emulsification (5 s every 5 min) was applied to nos. 1, 2, 5 and 6. NA, not applicable. ^aA flow of H₂ at atmospheric pressure was maintained during the reaction. ^bConversions and product yields were determined by GC–FID. Reminder: under standard conditions (Fig. 3c), \bar{j} = –78.0 mA, EB yield = 95.1%, FE_{EB} = 95.0%, FE_{H₂} = 1.2%.

at the top of the dispersion system, forming a dense ‘emulsion’ phase. After reaching a maximal magnitude of around –90 mA at 2 min, which presumably corresponds to the time needed for the macroscopic creaming process to take place (Supplementary Fig. 13), current magnitude decreased slowly, probably owing to mass transfer limitation of protons in the emulsion phase, until in situ emulsification initialized a new cycle. Thus, the creaming process plays a key role in electrical connectivity within the emulsion phase, and periodical in situ emulsification is required to avoid mass transfer limitations and maintain high performance (Supplementary Fig. 14). Interestingly, narrowing the Ag foil from 5 to 1 cm² did not affect substantially the rate of ECH (Supplementary Fig. 15), which shows that the area of the current collector is not a limiting factor. Taken together, these results strongly support the idea that ECH occurs at oil–water interfaces.

Investigation of emulsions in the ECH process

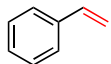
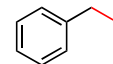
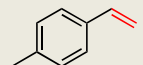
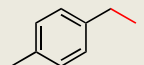
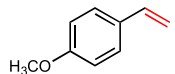
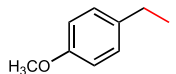
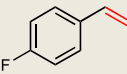
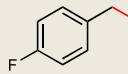
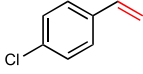
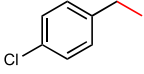
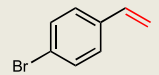
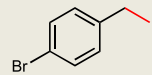
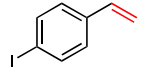
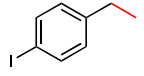
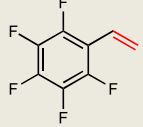
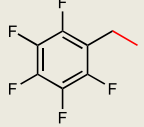
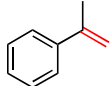
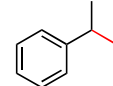
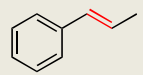
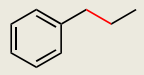


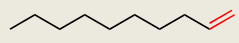
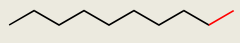
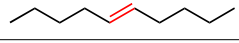
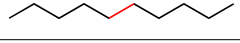
To gain a clearer understanding of the role of emulsions played in the ECH system, a series of control experiments was performed. First, electrolysis in the absence of a Pd/CNT catalyst but with placing of the Ag foil at the oil–water interface (Table 1, no. 1) produced trace amounts of EB despite a current of larger magnitude (–339.8 mA), although directed towards H₂ (FE_{H₂} = 94.9%). Therefore, a direct styrene ECH at the Ag foil can be ignored in the emulsion system, further corroborating the catalytic role played by Pd/CNTs at biphasic interfaces. Next, an emulsion system including molecularly modified CNTs(+) lacking Pd NPs (Table 1, no. 2) yielded only 0.6% of EB. This result demonstrates the poor activity of metal-free CNTs(+) for styrene ECH and confirms that Pd nanoparticles are responsible for the high electrocatalytic activity in Pd/CNTs(+)-stabilized emulsion ECH systems. The third control experiment was performed using Pd/CNTs(+) without emulsification (Table 1, no. 3) and thus dispersed in the aqueous phase. In this

configuration, 22.0% of EB yield and 21.9% of FE_{EB} were achieved, substantially lower than with the emulsified system. Moreover, conventional single-phase electrolysis was tested, for which styrene was solubilized in the electrolyte using ethanol as cosolvent and the cathode—made of Pd/CNTs(+)—coated directly onto the Ag foil (Table 1, no. 4). Electrolysis showed higher current compared with the typical emulsion system (–102.5 versus –78.0 mA), but was mostly directed towards HER (FE_{H₂} = 79.4%) and only poorly towards EB production (<20% yield and FE_{EB}). These results indicate that HER dominated the reaction pathway in the single-phase system, suggesting that the biphasic interfacial environment around Pd/CNTs(+) is crucial to favouring hydrogenation over HER.

To test thermochemical hydrogenation activity in the absence of applied potential, the emulsion phase was saturated with pure H₂ by maintaining a H₂ flow through the headspace while keeping other conditions unchanged (Table 1, no. 5). Under these conditions, the EB yield in Pd/CNTs(+)-stabilized emulsions reached 40.0%, defining an upper limit for the potential contribution of ‘classical’ hydrogenation using H₂ in the emulsion system (H₂ concentration in the headspace was <3 vol% during our standard electrocatalytic ECH, versus 100 vol% in this reference experiment). In Pd/CNTs(–)-stabilized emulsions a similar yield (42.3%) was obtained, indicating that the variation in performance of Pd/CNTs(+) and Pd/CNTs(–) in emulsion ECH did not originate from variation in their thermal catalytic activity.

The final control experiment (Table 1, no. 6) was performed in the presence of pure H₂ in the headspace while applying potential (–0.65 V_{RHE}) to the emulsion system, to identify any contribution of electrochemically promoted catalytic hydrogenation to styrene conversion. Following 50% of charge input (193 C), yields of EB (49.5%) and FE_{EB} (98.8%) were found to be very similar to those obtained under standard conditions without H₂ after the same charge input,

Table 2 | Hydrogenation of various alkenes using the emulsion ECH system

$R^1-CH=CH-R^2 \xrightarrow[-0.65 V_{RHE}, R.T.]{5 \text{ wt\%Pd/CNTs}(+)} R^1-CH_2-CH_2-R^2$ <div style="display: flex; justify-content: space-around; width: 100%;"> S SH_2 </div>						
Entry	Substrate	Product	Conversion (%) ^a	Yield (%) ^a	FE _{SH₂} (%)	$j_{Pd}^{SH_2}$ (mA mg _{Pd} ⁻¹)
1			96.5	96.5	96.5	-150.9
2			99.1	99.1	98.9	-121.5
3			92.1	92.1	92.0	-102.1
4			83.2	83.2	83.8	-186.2
5			99.0	99.0 (86.0) ^b	98.0	-151.6
6			33.0	33.0	32.8	-45.6
7			0.2	0.2	0.2	-0.3
8			57.4	57.4	57.3	-58.6
9			95.9	95.9	95.9	-99.5
10			87.4	87.4	87.2	-135.5
11			92.8	92.8	92.8	-254.0
12			76.0	44.6 ^c	44.5	-35.0
13			0	-	-	-

Reaction conditions: 2 mmol substrate, 10 mg of catalyst (Pd/CNTs(+), 4.7 μmol Pd), 10 ml of cyclohexane, 0.5 M H₂SO₄, room temperature, 386 C of electric charge; emulsification frequency, 5 s every 5 min. ^aConversions and product yields determined by GC-FID. ^bIsolated yield. ^cOther products are decene isomers.

indicating that electrochemically promoted catalytic hydrogenation plays a negligible role in our emulsion system. This conclusion was further reinforced by performing the reaction under D₂ (-0.65 V_{RHE}), in which no substantial incorporation of deuterium in EB was observed (Supplementary Figs. 16 and 17). We thus conclude, for our emulsion ECH system, that the intermediate formation of H₂ as a hydrogenation agent is bypassed. These results exclude mechanisms based on electrochemically promoted thermal hydrogenation under our conditions, and show that the hydrogenation process is indeed electrochemical in nature.

With our applied potential being far above the standard potential of the styrene⁻/styrene couple ($E^0 = -2.58$ V versus saturated calomel electrode (SCE))³², this rules out the occurrence of outer-sphere electron transfer to styrene generating freely diffusing radical styrene⁻ species. The absence of traceable amounts of radical coupling products (see above) corroborates this point and suggests more generally that long-lived radical intermediates are not formed during the process. We thus disfavour mechanistic hypotheses where electron and proton transfers to styrene would be separated (for example, in different

phases) because these pathways would lead to polymerization products. Then, using neat styrene as the oil phase, we found that current saturation occurs at potentials more negative than $-0.75 V_{\text{RHE}}$ (Supplementary Fig. 18). This point indicates that the diffusion of substrates (styrene or proton) is probably not limiting at our standard applied potential ($-0.65 V_{\text{RHE}}$). Furthermore, we observed that selectivity to EB remains close to unity and $j_{\text{Pd}}^{\text{EB}}$ remains within the same order of magnitude (in the range -100 to $-200 \text{ mA mg}_{\text{Pd}}^{-1}$), while the concentration in styrene spans almost more than two orders of magnitude (0.2 M to neat; Supplementary Table 2). These observations are consistent with an apparent 0th order in styrene observed for the formation of EB (Fig. 3c). We also found that the Hammett plot obtained using various *para*-substituted styrene substrates (see below) shows a very modest slope (Supplementary Fig. 19). These results collectively suggest that, under our standard conditions, the diffusion of styrene is not limiting and that it has little influence on rate determination. Experiments with D_2O rather than H_2O show a minor normal kinetic effect (Supplementary Fig. 20a) and confirm that H_2O (in our standard aqueous electrolyte) is the source of protons for the hydrogenation reaction (Supplementary Figs. 21 and 22). We thus propose that hydride formation or transport at the interface may be rate determining, which would point to an ECH mechanism that involves the transfer of adsorbed hydrides to the styrene substrate. Finally, the observed marked pH dependence of $j_{\text{Pd}}^{\text{EB}}$ and FE_{EB} (Supplementary Fig. 20b) can be explained by either a switch in mechanism or an alteration of ECSA with pH. We stress, however, that the intrinsic dependence of the physical properties of the emulsion on the nature and concentration of substrates renders mechanistic deconvolution highly challenging and prevents conclusive evidence in that regard.

We also demonstrate here that $j_{\text{Pd}}^{\text{EB}}$ of the emulsion ECH system can be further enhanced at a cost of slight compromise in regard to FE_{EB} (Supplementary Fig. 23). For example, $j_{\text{Pd}}^{\text{EB}}$ increased to $-368.7 \text{ mA mg}_{\text{Pd}}^{-1}$ when ECH was performed at $-1.05 V_{\text{RHE}}$, with FE_{EB} slightly decreased to 87.1%, presumably because the production rate of hydride from protons in the aqueous phase exceeded its consumption rate in the oil phase. Alternatively, maintaining the working potential at $-0.65 V_{\text{RHE}}$ while adding an additional proton source (2 mmol octanoic acid) in the oil phase also resulted in enhancement of $j_{\text{Pd}}^{\text{EB}}$ to $-240.1 \text{ mA mg}_{\text{Pd}}^{-1}$ at $\text{FE}_{\text{EB}} = 92.5\%$ (Supplementary Fig. 23). This increased activity with added octanoic acid is consistent with the potential involvement of protons in rate determination under our conditions. We also note that octanoic acid may play the role of a 'proton shuttle' by fostering the transfer of protons at the interface. Moreover, the emulsion ECH system performed similarly well when reducing the amount of Pd/CNTs(+) (Supplementary Fig. 24). These results illustrate the huge potential of the emulsion ECH system working at high current density while maintaining excellent FE.

Substrate compatibility

The versatility of the emulsion ECH system was explored by extending substrate scope to other styrene derivatives and alkenes with a standard concentration of 0.2 M in the oil phase. Encouragingly, excellent yields, FE (FE_{SH_2}) and specific current density ($j_{\text{Pd}}^{\text{SH}_2}$) were observed for styrene derivatives possessing electron-donating or -withdrawing groups in *para* position (Table 2, entries 2–6). In the case of the monohalogen-substituted styrene derivatives (entries 4–7), no dehalogenation was observed. The magnitude of $j_{\text{Pd}}^{\text{SH}_2}$ decreased across the halogen group ($\text{F} > \text{Cl} > \text{Br} \gg \text{I}$). Interestingly, ECH of 4-fluorostyrene (entry 4) proceeded at a $j_{\text{Pd}}^{\text{SH}_2}$ notably magnified compared with that of styrene derivatives having electron-donating groups, although at a slightly lower yield and FE_{SH_2} . While FE_{H_2} and yields were still excellent for 4-chlorostyrene (entry 5), both were reduced for 4-bromostyrene and 4-iodostyrene (entries 6 and 7, respectively), presumably due to unstable emulsions. The ECH product of 4-chlorostyrene was also successfully isolated after the reaction by filtering off Pd/CNTs(+), separating the organic phase and evaporating the solvent, from which we

obtained 1-chloro-4-EB at 86% yield (see Supplementary Fig. 25 for ^1H and ^{13}C NMR spectra). Going from a monofluorinated phenyl ring (4-fluorostyrene, entry 4) to a perfluorinated one (2,3,4,5,6-pentafluorostyrene, entry 8) markedly slowed conversion. α - and β -Methylstyrene were readily hydrogenated, giving the corresponding products at high yield, FE and $j_{\text{Pd}}^{\text{SH}_2}$ (entries 9–11). Interestingly, very high $j_{\text{Pd}}^{\text{SH}_2}$ was observed for the aliphatic alkene norbornene, at excellent yield and FE_{SH_2} . In contrast, poor performance was found with 1-decene, for which incomplete conversion, several isomers and large amounts of H_2 (0.6 mmol, 30% FE_{H_2}) were observed (entry 12). In this case, hydrogenation of the terminal double bond probably competed with isomerization to internal positions, which are generally harder to hydrogenate. Starting from trans-5-decene (entry 13) resulted in no conversion (neither hydrogenation nor isomerization), confirming that long-chain aliphatic alkenes—and especially internal ones—are challenging to hydrogenate using this system.

Conclusions

To summarize, we developed here a Pickering emulsion system efficient in the ECH of organic substrates with low water solubility. Molecular functionalization was employed to generate positively charged CNTs, which we used as support for catalytically active Pd nanoparticles. The resulting Pd/CNTs(+) material acted as both stabilizer for Pickering emulsions and electrocatalyst located at oil–water interfaces. The design benefits simultaneously from the high ionic conduction and proton concentration of the acidic aqueous electrolyte and the solubilization of substrates in the oil phase. During reaction, positively charged emulsion droplet interfaces electrically connect to the negatively charged Ag current collector and act as an extended cathode. Taking styrene as a model substrate, the emulsion ECH system showed current density as high as $-148.1 \text{ mA mg}_{\text{Pd}}^{-1}$ with FE to EB close to unity. As compared with state-of-the-art Pd membrane reactors, this system offers an improvement in hydrogenation FE, by 30–50%, at Pd-normalized specific current densities one order of magnitude higher. The performance of the emulsion ECH system was also observed for many other water-insoluble alkenes. Simple, versatile and efficient, this approach opens the way for the practical application of ECH to a wide range of water-insoluble organic substrates.

Methods

Pretreatment of CNTs

The detailed preparation process can be found in the literature²⁶. Briefly, pristine CNTs were treated with a mixture of nitric acid and sulfuric acid (1:1, nitric acid 65% and sulfuric acid 98%) to remove metal impurities and generate oxygen-containing functionalities on the CNT surface. In a typical procedure, pristine CNTs (10 g) were suspended in 500 ml of the acid mixture and heated at 105°C for 4 h. The solid product was then washed several times with ultrapure water and dried at 100°C for 20 h. The resulting product is CNTs(–).

Molecular modification of CNTs

Molecular modification of CNTs was carried out under argon using standard Schlenk techniques. Specifically, in a Schlenk tube CNTs(–) (200 mg) were added to thionyl chloride (4 ml, 55.2 mmol) and the resulting mixture was stirred at 30°C for 3 h. Thionyl chloride was then removed under vacuum. Histamine dihydrochloride (172 mg, 0.94 mmol), anhydrous Dimethylformamide (DMF, 6 mL) and 1,8-Diazabicyclo[5.4.0]undec-7-ene (DBU, 0.4 ml) were mixed in a small vial, yielding a clear solution. This solution was added to the Schlenk tube containing the CNTs and the mixture was stirred at 60°C for 5 h. Afterwards, CNTs were washed three times with an acetone:water (8:2) mixture using a centrifuge and dried under vacuum. Then, (3-bromopropyl)trimethylammonium bromide (245 mg, 0.94 mmol) and DMF (10 ml) were added to dried CNTs and the mixture was stirred at 80°C for 6 h. After cooling and washing three times with acetone:water

(8:2), the resulting CNTs were redispersed in 15 ml of acetone water (8:2) and LiNTf_2 (270 mg, 0.94 mmol) was added. The mixture was stirred at room temperature overnight, and CNTs(+) were collected after washing three times with acetone:water (8:2) and drying.

Pd colloid preparation

A colloidal solution of Pd NPs was prepared by adaptation of a previously reported method³⁶. Typically, in a Schlenk tube under argon flow, $\text{Pd}(\text{acac})_2$ (75 mg, 0.25 mmol) was mixed with oleylamine (15 ml) and stirred at 60 °C, resulting in a near-colourless solution. Borane triethylamine (300 mg, 2.61 mmol) was solubilized in oleylamine (4 ml) and the resulting solution immediately injected into the Pd-oleylamine solution at 60 °C. The temperature was then increased to 90 °C for 60 min. After reaction, the mixture was cooled to room temperature and 30 ml of ethanol added. The solid product was collected by centrifugation, redispersed in 2 ml of hexane and stored at 4 °C for future use.

Deposition of Pd nanoparticles on CNTs

Pd NPs were deposited on CNTs(–) or CNTs(+) with 5 wt% loading. In a typical protocol, CNTs(+) (100 mg) were well dispersed in a mixture of hexane:isopropanol (7:3, 10 ml) by sonication. Next, 385 μl of pre-prepared Pd NP colloidal solution (containing 5 mg Pd) was diluted in 2 ml of hexane and added to the CNTs(+) dispersion. The mixture was further sonicated for 30 min and then left to stand for 1 h. The resulting solid product was washed once by acetic acid and three times by hexane. Finally, the product was dried under vacuum to obtain the electrocatalyst.

Electrochemical set-up and typical protocol

The electrolysis cell used in this work was customized in the workshop of our institute. The cell consists of two compartments separated by a glass frit, with an in situ homogenizer installed on top of the cathode compartment. Pickering emulsions were filled in the cathode compartment while the reference electrode (RE; AgCl/Ag, saturated KCl) and the counter electrode (CE; Pt wire) were inserted in the anode compartment. During reaction, the homogenizer was intermittently switched on and off by a digital timer at a frequency of 5 s per 5 min. Before performing electrohydrogenation, an air-tightness test was conducted based on water electrolysis. As shown in Supplementary Fig. 26b, the detected level of H_2 is in agreement with the theoretical value expected from the charge input, which indicates a good tightness of the cell.

In a typical protocol, the electrocatalyst (10 mg, 4.7 μmol Pd) and H_2SO_4 (10 ml, 0.5 M) were mixed in a 20 ml vial and dispersed by sonication while styrene (2 mmol) was dissolved in cyclohexane (10 ml) in another 20 ml vial. A H_2SO_4 solution (65 ml, 0.5 M) filled the anode compartment while electrocatalyst dispersion and styrene solution were added to the cathode compartment. The mixture in the cathode compartment was then emulsified by the homogenizer for 2 min to generate Pickering emulsions. The headspace of the cell was purged with an Ar flow (50 ml min^{-1}) for 10 min. After sealing all ports, REs and CEs were inserted in the anode compartment and the electrolysis was started. Electrolysis was recorded in potentiostatic mode at $-0.65 V_{\text{RHE}}$ with ohmic drop (iR) compensation in all cases. During electrolysis, the electrolyte in the anode compartment was magnetically stirred at 300 r.p.m. while the emulsion in the cathode compartment was emulsified at a frequency of 5 s every 5 min; a thin spiral needle (0.4 mm) piercing the rubber septum of the sampling port acted as a check valve to release pressure in the cell. After a certain time interval, 0.5 ml of emulsion was sampled and analysed by gas chromatography with a flame ionization detector (GC–FID) using tetradecane as internal standard. The headspace was analysed by GC–TCD using an autosampler (sampling volume 0.4 ml). For electrolysis performed at $-1.05 V_{\text{RHE}}$, the emulsification frequency was 5 s every 2 min.

Preparation of Ag foil coated with Pd/CNTs(+)

Pd/CNTs(+) (10 mg) were dispersed in 1 ml of isopropanol by sonication to obtain a ‘catalyst ink’. This ink was then carefully dropped onto the slowly rotating Ag current collector to enable it to cover a greater surface area. After the first drop had dried, the coating process was repeated until the entire Ag surface was covered and all the ink used up. Afterwards, the current collector was placed in an oven at 70 °C for 30 min to fully remove the solvent, and was then used for electrocatalysis testing.

pH variation

To conduct electrolyses at varying pH, the pH of the electrolyte was set by the addition of sulfuric acid or sodium hydroxide and the ion strength of the solution kept constant by the addition of sodium sulphate. Reactions were stopped after a charge input of 19.3 C.

RE calibration

The RE used in this work is a AgCl/Ag (saturated KCl) electrode. The potential of the RE was calibrated versus the $[\text{Fe}(\text{CN})_6]^{3-}/[\text{Fe}(\text{CN})_6]^{4-}$ couple in an electrolysis cell. Calibration was performed in 0.1 M potassium phosphate buffer (pH 7.0), with a glassy carbon electrode (0.07 cm^2) and a platinum wire as the WE and CE, respectively. The conversion of potentials against the normal hydrogen electrode (NHE) potential was achieved using the following equation: $E_{\text{AgCl/Ag versus NHE}} = E_{\text{Fe(III/II) versus NHE}} - E_{\text{Fe(III/II) versus AgCl/Ag}}$. Here, $E_{\text{Fe(III/II) versus AgCl/Ag}}$ and $E_{\text{Fe(III/II) versus NHE}}$ (0.425 V) represents the potential value for the $[\text{Fe}(\text{CN})_6]^{3-}/[\text{Fe}(\text{CN})_6]^{4-}$ couple determined experimentally versus the AgCl/Ag RE and tabulated against the NHE, respectively³⁷. A conversion value of $E_{\text{AgCl/Ag versus NHE}} = 128 \text{ mV}$ was found. AgCl/Ag RE used in this work has a potential of 146 mV versus RHE (abbreviated V_{RHE} in the following) (0.5 M H_2SO_4 , pH 0.3).

E_{pzc} measurement of Ag foil

This measurement was performed in 0.5 M H_2SO_4 electrolyte with Ag foil (0.5 cm^2), a platinum wire and a AgCl/Ag electrode as the WE, CE and RE, respectively. Electrochemical impedance spectroscopy was recorded at different potential scanning frequencies, from 100 kHz to 100 MHz, with 20 points recorded per decade. The obtained spectra were fitted using the circle-fitting tool in EC-Lab software (BioLogic) to obtain the capacitance of the Ag foil at each potential. After plotting capacitance versus potential (Fig. 3d), the potential corresponding to the lowest capacitance value represents E_{pzc} of Ag foil. In our work, this value was measured at around -0.49 to $-0.52 V_{\text{RHE}}$, slightly lower than that reported in the literature³⁵.

Double-layer capacitance measurement

Cyclic voltammetry scans were recorded at four scan rates with a minimum of three cycles in the non-faradaic region, specifically between 146 and 96 mV_{RHE} . Scan rates of 50, 100, 200 and 400 mV s^{-1} were used. The difference in currents at 121 mV_{RHE} between forward and reverse scans of the second cycle was plotted against the scan rate. The slope of an affine fitting of the resulting plots gives access to the capacitance of the cathode electric double layer, which is proportional to the ECSA of the cathode.

Data availability

Data that support the findings of this study, including material characterizations and catalytic measurements, are available within the paper and its Supplementary Information files. Further requests about data can be directed to the corresponding authors.

References

1. Panwar, N. L., Kaushik, S. C. & Kothari, S. Role of renewable energy sources in environmental protection: a review. *Renew. Sust. Energy Rev.* **15**, 1513–1524 (2011).

- Jiayi, H., Chuanwen, J. & Rong, X. A review on distributed energy resources and MicroGrid. *Renew. Sust. Energy Rev* **12**, 2472–2483 (2008).
- Badwal, S. P. S., Giddey, S. S., Munnings, C., Bhatt, A. I. & Hollenkamp, A. F. Emerging electrochemical energy conversion and storage technologies. *Front. Chem.* **2**, 79 (2014).
- Akorede, M. F., Hizam, H. & Pouresmaeil, E. Distributed energy resources and benefits to the environment. *Renew. Sust. Energy Rev.* **14**, 724–734 (2010).
- De Luna, P. et al. What would it take for renewably powered electrosynthesis to displace petrochemical processes? *Science* **364**, eaav3506 (2019).
- Papanikolaou, G., Centi, G., Perathoner, S. & Lanzafame, P. Catalysis for e-chemistry: need and gaps for a future de-fossilized chemical production, with focus on the role of complex (direct) syntheses by electrocatalysis. *ACS Catal.* **12**, 2861–2876 (2022).
- Lucas, F. W. S. et al. Electrochemical routes for the valorization of biomass-derived feedstocks: from chemistry to application. *ACS Energy Lett.* **6**, 1205–1270 (2021).
- Yuan, Y. & Lei, A. Electrochemical oxidative cross-coupling with hydrogen evolution reactions. *Acc. Chem. Res.* **52**, 3309–3324 (2019).
- Akhade, S. A. et al. Electrocatalytic hydrogenation of biomass-derived organics: a review. *Chem. Rev.* **120**, 11370–11419 (2020).
- De Arquer, F. P. G. et al. CO₂ electrolysis to multicarbon products at activities greater than 1 A cm⁻². *Science* **367**, 661–666 (2020).
- Sherbo, R. S., Delima, R. S., Chiykowski, V. A., MacLeod, B. P. & Berlinguette, C. P. Complete electron economy by pairing electrolysis with hydrogenation. *Nat. Catal.* **1**, 501–507 (2018).
- Sherbo, R. S., Kurimoto, A., Brown, C. M. & Berlinguette, C. P. Efficient electrocatalytic hydrogenation with a palladium membrane reactor. *J. Am. Chem. Soc.* **141**, 7815–7821 (2019).
- Dinh, C.-T. et al. CO₂ electroreduction to ethylene via hydroxide-mediated copper catalysis at an abrupt interface. *Science* **360**, 783–787 (2018).
- Iwakura, C., Yoshida, Y. & Inoue, H. A new hydrogenation system of 4-methylstyrene using a palladinized palladium sheet electrode. *J. Electroanal. Chem.* **431**, 43–45 (1997).
- Inoue, H., Abe, T. & Iwakura, C. Successive hydrogenation of styrene at a palladium sheet electrode combined with electrochemical supply of hydrogen. *Chem. Commun.* **1996**, 55–56 (1996).
- Huang, A. et al. Electrolysis can be used to resolve hydrogenation pathways at palladium surfaces in a membrane reactor. *JACS Au* **1**, 336–343 (2021).
- Delima, R. S., Sherbo, R. S., Dvorak, D. J., Kurimoto, A. & Berlinguette, C. P. Supported palladium membrane reactor architecture for electrocatalytic hydrogenation. *J. Mater. Chem. A Mater.* **7**, 26586–26595 (2019).
- Aveyard, R., Binks, B. P. & Clint, J. H. Emulsions stabilised solely by colloidal particles. *Adv. Colloid Interface Sci.* **100**, 503–546 (2003).
- Han, C. et al. Palladium/graphitic carbon nitride (g-C₃N₄) stabilized emulsion microreactor as a store for hydrogen from ammonia borane for use in alkene hydrogenation. *Angew. Chem. Int. Ed. Engl.* **57**, 14857–14861 (2018).
- Han, C., Xu, H., Waclawik, E., Li, X.-H. & Xu, J. A bioinspired microreactor with interfacial regulation for maximizing selectivity in a catalytic reaction. *Chem. Commun.* **56**, 8059–8062 (2020).
- Zhang, M. et al. Compartmentalized droplets for continuous flow liquid-liquid interface catalysis. *J. Am. Chem. Soc.* **138**, 10173–10183 (2016).
- Zhang, M. et al. Ionic liquid droplet microreactor for catalysis reactions not at equilibrium. *J. Am. Chem. Soc.* **139**, 17387–17396 (2017).
- Kurimoto, A. et al. Physical separation of H₂ activation from hydrogenation chemistry reveals the specific role of secondary metal catalysts. *Angew. Chem. Int. Ed. Engl.* **60**, 11937–11942 (2021).
- Mi, X. et al. Modified reduced graphene oxide as stabilizer for Pickering w/o emulsions. *J. Mater. Sci.* **55**, 1946–1958 (2020).
- He, Y. et al. Factors that affect Pickering emulsions stabilized by graphene oxide. *ACS Appl. Mater. Interfaces* **5**, 4843–4855 (2013).
- Ding, Y. et al. Dynamic carbon surface chemistry: revealing the role of carbon in electrolytic water oxidation. *J. Energy Chem.* **47**, 155–159 (2020).
- Cao, Y., Lai, Z., Feng, J. & Wu, P. Graphene oxide sheets covalently functionalized with block copolymers via click chemistry as reinforcing fillers. *J. Mater. Chem.* **21**, 9271–9278 (2011).
- Bordet, A. et al. Molecular control of the catalytic properties of rhodium nanoparticles in supported ionic liquid phase (SILP) systems. *ACS Catal.* **10**, 13904–13912 (2020).
- Seo, S., Park, J. & Kang, Y.-C. Chemical analysis of ionic liquids using photoelectron spectroscopy. *Bull. Korean Chem. Soc.* **37**, 355–360 (2016).
- Moulder, J. F. Handbook of X-ray Photoelectron Spectroscopy (Physical Electronics, 1995).
- Heard, D. M. & Lennox, A. J. J. Electrode materials in modern organic electrochemistry. *Angew. Chem. Int. Ed. Engl.* **59**, 18866–18884 (2020).
- Filardo, G., Gambino, S., Silvestri, G., Gennaro, A. & Vianello, E. Electrocarboxylation of styrene through homogeneous redox catalysis. *J. Electroanal. Chem. Interfacial Electrochem.* **177**, 303–309 (1984).
- Zebardast, H. R., Rogak, S. & Asselin, E. Potential of zero charge of glassy carbon at elevated temperatures. *J. Electroanal. Chem.* **724**, 36–42 (2014).
- Lica, G. C. & Tong, Y. J. Electrochemical impedance spectroscopic measurement of potential of zero charge of octanethiolate-protected Au and Pd nanoparticles. *J. Electroanal. Chem.* **688**, 349–353 (2013).
- Sato, N. In *Electrochemistry at Metal and Semiconductor Electrodes* (ed. Sato, N.) 119–199 (Elsevier Science, 1998).
- Mazumder, V. & Sun, S. Oleylamine-mediated synthesis of Pd nanoparticles for catalytic formic acid oxidation. *J. Am. Chem. Soc.* **131**, 4588–4589 (2009).
- O'Reilly, J. E. Oxidation-reduction potential of the ferro-ferricyanide system in buffer solutions. *Biochimica et Biophysica Acta Bioenerg.* **292**, 509–515 (1973).

Acknowledgements

We acknowledge financial support by the Max Planck Society and Deutsche Forschungsgemeinschaft, under Germany's Excellence Strategy – Exzellenzcluster 2186 'The Fuel Science Center', no. 390919832. A.B. thanks Max-Buchner-Forschungstiftung for funding (no. 3827). J.Z. thanks the networking programme 'Sustainable Chemical Synthesis 2.0' for support and fruitful discussions across disciplines. S. Heumann and Y. Ding are acknowledged for providing pretreated CNT material. We thank A. Jakubowski, A. Gurowski, J. Werkmeister, J.-T. Krzeslack and N. Pfänder (MPI-CEC) for support with analytics. Open access funding was provided by the Max Planck Society.

Author contributions

C.H. proposed the original idea, participated in the basic project definition and conceptual planning of the experimental work flow, performed experimental work and data interpretation and wrote the manuscript draft. J.Z. participated in experimental work, data interpretation and revision of the manuscript. J.J. analysed XPS data and wrote the corresponding section of the manuscript. N.K. participated in supervision of the experimental work, in data

interpretation and in writing of the manuscript. A.B. participated in the basic project definition and the conceptual planning of experimental work flow, supervised experimental work and contributed to data interpretation and writing of the manuscript. W.L. participated in data interpretation and writing of the manuscript.

Funding

Open access funding provided by Max Planck Society.

Competing interests

The authors declare no competing interests.

Additional information

Supplementary information The online version contains supplementary material available at <https://doi.org/10.1038/s41929-022-00882-4>.

Correspondence and requests for materials should be addressed to Nicolas Kaeffer or Alexis Bordet.

Peer review information *Nature Catalysis* thanks Mahito Atobe and the other, anonymous, reviewer(s) for their contribution to the peer review of this work.

Reprints and permissions information is available at www.nature.com/reprints.

Publisher's note Springer Nature remains neutral with regard to jurisdictional claims in published maps and institutional affiliations.

Open Access This article is licensed under a Creative Commons Attribution 4.0 International License, which permits use, sharing, adaptation, distribution and reproduction in any medium or format, as long as you give appropriate credit to the original author(s) and the source, provide a link to the Creative Commons license, and indicate if changes were made. The images or other third party material in this article are included in the article's Creative Commons license, unless indicated otherwise in a credit line to the material. If material is not included in the article's Creative Commons license and your intended use is not permitted by statutory regulation or exceeds the permitted use, you will need to obtain permission directly from the copyright holder. To view a copy of this license, visit <http://creativecommons.org/licenses/by/4.0/>.

© The Author(s) 2022